Effects of Film Forming Compounds on the growth of Giant CCN: Implications for cloud microphysics and the aerosol indirect effect.

JEESSY MEDINA[1] and ATHANASIOS NENES* [1, 2]

[1]School of Chemical & Biomolecular Engineering, Georgia Institute of Technology, Atlanta, Georgia

[2]Also in the School of Earth and Atmospheric Sciences, Georgia Institute of Technology, Atlanta, Georgia

Short title: Film forming compounds and Giant CCN

*Corresponding author

Abstract. The presence of Giant cloud condensation nuclei (GCCN) within stratocumulus clouds can help the formation of drizzle by acting as collector drops. We propose that the presence of Film Forming Compounds (FFCs) on GCCN may decrease their growth enough to cease this drizzle formation mechanism. We systematically explore the accommodation properties and amount of FFCs necessary to have a significant impact on GCCN size under realistic conditions of growth inside typical stratocumulus clouds. It is found that even low mass fractions (as low as 0.2%) of FFCs with a modest effect on water vapor accommodation can significantly reduce GCCN size and their potential to act as collector drops. Our conclusions apply to both pristine and polluted aerosol conditions, which suggest that in the presence of FFCs, GCCN may be influencing the microphysical evolution of clouds to a lesser extent than previously thought.

1. Introduction

Understanding aerosol-cloud interactions is a prerequisite for understanding the hydrological cycle and climate. Because cloud droplets form on pre-existing aerosols, also known as Cloud Condensation Nuclei (CCN), anthropogenic activities that increase aerosol concentrations may lead to more reflective clouds by increasing the amount of CCN. This phenomenon is known as the "first" aerosol indirect effect [*Twomey*, 1977]. High concentrations of CCN also may delay the formation of drizzle (the precursor of precipitation), which would increase cloud lifetime and cloud height; this is the so-called "second" aerosol indirect effect [*Albrecht*, 1989]. Any process that affects the formation of drizzle in clouds can be an important component of the "second" indirect effect. Marine environments, because of low CCN concentrations, are particularly susceptible to both indirect effects; in particular, marine stratocumulus clouds which contribute about a third of global cloud coverage [*Albrecht*, 1989].

Giant Cloud Condensation Nuclei (GCCN), CCN with dry particle diameters greater than 5 μm, can influence drizzle formation because they grow enough in-cloud to become efficient collector drops [*Johnson*, 1982; *Tzivion et al.*, 1994; *Cooper et al.*, 1997; *Feingold et al.*, 1999]. GCCN may be present in marine aerosol; number concentrations for particles in the Northeast Atlantic in the 5 - 150 μm range are between 0.1-0.5 cm^{-3} [Exton et al., 1986]. They are usually generated by breaking of surface waves, as well as other dynamically influenced mechanical processes [*Fitzgerald*, 1991 and references therein]. GCCN may also be of continental origin such as plant debris, or large dust particles [*Rudich et al.*, 2002 and references therein]. *Feingold et al.* [1999] showed that low concentrations (as low as 10^{-4} cm^{-3}) of GCCN are sufficient to transition marine stratocumulus clouds from a

non-drizzling to a drizzling state. The same study showed that GCCN become more efficient in initiating drizzle formation as CCN concentrations increase. This hypothesis is supported by observations from remote sensing data; *Rosenfeld et al*. [2002] showed that polluted clouds developing over the Indian Ocean tended to precipitate in contrast to polluted clouds that developed over the South Asian Continent. They concluded that precipitation was enhanced in the clouds over the Indian Ocean by the presence of GCCN generated from sea spray. Using the same remote sensing technique, *Rudich et al*. [2002] provided evidence that large salt-containing dust particles promoted precipitation in clouds downwind of the Aral Sea. The presence of GCCN may be a significant component of the "second" indirect effect, but is currently not included in climate models.

In addition to dust and salt, GCCN may contain significant amounts of organics and black carbon (BC) [*Lelieveld et al.*, 2001]. Under certain conditions, BC inclusions may absorb enough radiation to heat the GCCN and decrease its size to prevent it from acting as a collector drop [*Nenes et al.*, 2002b]. Furthermore, organic species may form hydrophobic films on the surface of GCCN. These films, often composed of fatty acids acquired from the air/ocean surface interface [*Tervahattu et al.*, 2002a; *Tervahattu et al.*, 2002b], may influence the growth of GCCN by decreasing the condensation rate of water onto them. It is quite likely that organics from anthropogenic emissions may also have the same effect. *Chuang* [2003] observed particles in Mexico City that exhibited significant growth delay. The delay was attributed to organic films on the surface of aerosols with an estimated mass accommodation coefficient ranging from 1×10^{-5} to 4×10^{-5}, more than two orders of magnitude less than that for pure water drops. The effect of organic films on the activation of CCN has been the focus of numerous studies [e.g., *Gill et al.*, 1983; *Shulman et al.*, 1997;

Cruz and Pandis, 1998; *Feingold and Chuang,* 2002]; all agree that additional information is needed to describe the effect of organics on the water uptake of CCN.

As stated, the presence of GCCN can enhance the formation of drizzle. However, it is possible that the presence of Film Forming Compounds (FFCs) on GCCN may delay their growth such that the latter became too small to act as efficient collector drops; hence, this mechanism of drizzle formation may cease. The potential effect of FFCs on GCCN growth and its implications for cloud precipitation processes are addressed in this study. Through simulations of GCCN growth within stratocumulus clouds, we define a range of accommodation properties and organic mass fractions necessary for FFCs to impart important reductions in GCCN size. Slow growth kinetics attributable to the dissolution of partially soluble substances [*Shulman et al.,* 1996; *Shantz et al.,* 2003] may also affect GCCN growth, but is beyond the scope of this study.

2. Model Formulation

The growth of GCCN within a stratocumulus cloud is simulated using the Trajectory Ensemble Model (TEM) approach of *Stevens et al.* [1996]. This methodology employs a Large Eddy Simulation (LES) of a cloud field that generates a set of Lagrangian trajectories that describe the evolution of the cloud field. Each trajectory within the set forces a non-adiabatic parcel model that calculates the growth of a GCCN. A horizontal ensemble average GCCN size throughout the boundary layer is calculated.

2.1 Model equations: Trajectory properties and supersaturation profiles. Each trajectory contains variables that characterize the thermodynamic state of a material point, as it is advected throughout the flow field. The variables contained in the trajectories are time *t*, position *x*, *y*, and *z*, pressure *p*, potential temperature in moist air θ_l, and the total (e.g. liquid

and vapor) water mass mixing ratio, w_t. The time step between two consecutive trajectory points is 2 s. All material points are initially taken below cloud level to ensure that their initial liquid water content (LWC) is approximately zero. The tendencies of *x*, *y*, *z*, *p*, θ_l, and w_t are calculated by the finite difference between two consecutive time steps.

Calculation of the growth of GCCN within a trajectory requires the knowledge of the parcel *p*, temperature *T*, and the parcel water vapor supersaturation, *S*. This is not directly available from the trajectories, and is calculated as follows. T is computed from θ_l, defined as:

$$\theta_l = T\left(\frac{p_o}{p}\right)^{\frac{C_p}{R}} + \frac{\Delta H_v}{C_p}\left(\frac{p_o}{p}\right)^{\frac{C_p}{R}} w_l \tag{1}$$

where ΔH_v is the latent heat of vaporization of water, C_p is the molar heat capacity of air, w_l is the liquid water mass mixing ratio, p_o is the reference pressure (1000 mb), and R is the universal gas constant. Equation 1 is used to solve for *T* and its rate of change, dT/dt:

$$T = \theta_l\left(\frac{p}{p_o}\right)^{\frac{C_p}{R}} - \frac{\Delta H_v}{C_p} w_l \tag{2}$$

$$\frac{dT}{dt} = \left(\frac{p}{p_o}\right)^{\frac{C_p}{R}} \frac{d\theta_l}{dt} + \theta_l\left(\frac{1}{p_o}\right)^{\frac{C_p}{R}}\left(\frac{C_p}{R}\right) p^{\frac{C_p}{R}-1}\frac{dp}{dt} + \frac{\Delta H_v}{C_p}\frac{dw_l}{dt} \tag{3}$$

$d\theta_l/dt$ and dp/dt from Equation 3 are approximated using $\Delta\theta_l/\Delta t$ and $\Delta p/\Delta t$ from the trajectory output.

S is calculated from the water vapor mass mixing ratio, w_v [*Seinfeld and Pandis*, 1998],

$$S = \frac{w_v}{w_v^*} = \frac{pM_a}{p^\circ M_w} w_v \tag{4}$$

where w_v^* is the saturation water vapor mixing ratio, M_w and M_a are the molar masses of water and air, respectively. w_v is calculated from the conservation of water in the parcel:

$$w_t = w_v + w_l \tag{5}$$

Solving for the rate of change of w_v and using the trajectory output $\Delta w_t / \Delta t$ for dw_t / dt, we obtain:

$$\frac{dw_v}{dt} = \frac{dw_t}{dt} - \frac{dw_l}{dt} \approx \frac{\Delta w_t}{\Delta t} - \frac{dw_l}{dt} \tag{6}$$

The liquid condensation rate is calculated as [*Seinfeld and Pandis*, 1998],

$$\frac{dw_l}{dt} = \frac{\pi}{2} \sum_i N_i D_{p_i}^2 \rho_w \frac{dD_{p_i}}{dt} \tag{7}$$

where N_i is the number of droplets (in each size class) per unit mass of air, ρ_w is the density of water, D_{p_i} is the droplet diameter of each size class. The growth/evaporation rate of each droplet is given by [*Seinfeld and Pandis*, 1998],

$$\frac{dD_{p_i}}{dt} = \left[\frac{\rho_w RT}{4p^\circ D_v' M_w} + \frac{\Delta H_v \rho_w}{4k_a' T} \left(\frac{\Delta H_v \rho_w}{TR} - 1 \right) \right]^{-1} \frac{1}{D_{p_i}} \left(S - S_{eq} \right) \tag{8}$$

where S_{eq} is the water vapor saturation ratio of the droplet. Köhler theory describes S_{eq} [*Seinfeld and Pandis*, 1998],

$$\ln\left(S_{eq}\right) = \frac{A}{D_p} - \frac{B}{D_p^3} \tag{9}$$

$$A = \frac{4M_w \sigma}{RT\rho_w} \tag{10}$$

$$B = \frac{6 n_s M_w}{\pi \rho_w} \tag{11}$$

where σ is the droplet surface tension, and n_s is the moles of solute dissolved in the droplet. The water vapor diffusivity, $D_v^{'}$, and the thermal conductivity of air, $k_a^{'}$, (both modified to account for non-continuum effects) are given by,

$$D_v^{'} = \frac{D_v}{1 + \frac{2 D_v}{\alpha D_p}\left(\frac{2\pi M_w}{RT}\right)^{\frac{1}{2}}} \tag{12}$$

$$k_a^{'} = \frac{k_a}{1 + \frac{2 k_a}{\alpha_T D_p \rho_a C_p}\left(\frac{2\pi M_a}{RT}\right)^{\frac{1}{2}}} \tag{13}$$

where α and α_T are the mass and thermal accommodation coefficients, respectively, and ρ_a is the density of air. We assume that α_T is equal to unity, and the presence of FFCs bears no effect on the parameter. (Although not explored here, if there were an effect, α_T would decrease and further delay droplet growth). The non-modified water vapor diffusivity, D_v, and the thermal conductivity of air, k_a, are given by:

$$D_v = \frac{0.211 \times 10^5}{p}\left(\frac{T}{273}\right)^{1.94} \tag{14}$$

$$k_a = 10^{-3}(4.39 + 0.071 * T) \tag{15}$$

To summarize, *T*, *p*, and *S* within the air parcel are calculated from the LES trajectories in the following manner. Initial conditions for θ_l, *p*, and w_t are used to calculate the initial value of T, assuming that w_l is negligible. The initial *S* is calculated using Equation 4. The initial D_{p_i} are calculated assuming the aerosol is in equilibrium with S.

The derivatives of θ_l, p, w_t with respect to time are obtained from the trajectory output, and the parcel T, p, and S are obtained by integrating Equations 3, 6, 7 and 8 using the implicit ODE solver LSODE [*Hindmarsh*, 1983].

2.2 CCN populations. Two supersaturation histories, one characteristic of a pristine and one of a urban environment, were derived for each LES trajectory set. The marine and urban aerosol size distributions of *Whitby* [1978] are used to represent the aerosol populations for the pristine and polluted environments, respectively (Table 1). Polluted clouds tend to have lower supersaturations relative to their pristine counterparts, because of the increased competition in the latter for water vapor (e.g., *Nenes et al.*, 2001). As a result, the driving force for GCCN growth in polluted clouds is smaller compared to that of pristine clouds thus GCCN may have less probability of becoming collector drops.

When calculating the supersaturation levels, a simple chemical composition (ammonium sulfate) is assumed for the aerosol. In reality, the presence of FFC-containing GCCN should coincide with the presence of FFCs throughout the aerosol size distribution. However, since we consider two extreme CCN conditions (pristine vs. urban), it is rather unlikely to imagine a condition of FFC-coated aerosol that would yield supersaturation levels outside of the two cases. Thus, the simplified aerosol chemical composition is sufficient for our study.

2.3 GCCN size calculations. Figure 1 illustrates the procedure used in calculating the growth of GCCN within a stratocumulus cloud. The Lagrangian trajectories were obtained from the LES simulation and used in conjunction with either pristine or polluted aerosol populations as inputs into the cloud parcel model described in Section 2.1. The parcel model computes a supersaturation history for each of the trajectories. Along each

trajectory, droplets are subject to a uniform "macroscopic supersaturation"; we neglect considering that individual droplets might be subject to local fluctuations that persist down to the millimeter scale, as we already consider two drastically different supersaturation regimes (marine vs. urban CCN conditions); we presume that smaller-scale fluctuations lie within this range. GCCN with a prescribed chemical composition are grown (according to Equation 8) using the supersaturation profiles calculated for each trajectory. The temporal (1hr) and horizontally-averaged GCCN size is then calculated to represent the average vertical profiles of GCCN size.

3. Simulations

3.1 Stratocumulus Clouds. Lagrangian trajectories used in this study were derived from two marine stratocumulus cloud simulations ("ASTEX-1" and "ASTEX-2") for conditions observed during the Atlantic Stratocumulus Transition Experiment [*Albrecht et al.*, 1995]. 500 trajectories covering 1 hour of simulation time were derived for each cloud. Figures 2a and 2b display important characteristics for each cloud. ASTEX-1 and ASTEX-2 have average updraft velocities of about 0.2 to 0.4 m s^{-1}, respectively; both clouds are energetic enough to maintain droplets of at least 80 μm in diameter. ASTEX-2 is a heavily drizzling cloud with a higher LWC (0.6 g m^{-3}) and lower cloud base (200 m) than ASTEX-1 (0.4 g m^{-3} and 400 m, respectively).

3.2 Composition and size of GCCN. We consider GCCN composed of soluble and insoluble material with an average density of 1760 kg m^{-3}. The soluble material is assumed to be $(NH_4)_2SO_4$ and the insoluble fraction is treated as a mixture of FFCs and core material. We consider initial dry CCN diameters, $D_{p,dry}$, of 1 μm, 2.5 μm, 5 μm, 7.5 μm, 10 μm, 12.5

μm, 15 μm, and 25 μm. For each particle size, simulations were performed for different soluble mass fractions, ε_s, of 25%, 50%, and 75%. Finally, for each ε_s, the FFC mass fraction, ε_o, was varied from 0.2% to 20%. A total of 2016 simulations were done for the ASTEX-1 and ASTEX-2 trajectory sets.

3.3 FFCs and their effect on droplet growth rate. We adopt a "film-breaking" model [*Feingold and Chuang*, 2002] to describe the effect of FFCs on droplet growth rate (Figure 3). When present, FFCs are initially assumed to form a film on the CCN surface. This makes the particle experience slow growth, expressed by a low value of the accommodation coefficient, α_{slow}. If the particle grows enough to break its film, the FFCs are incorporated within the insoluble core material. The droplet surface becomes an aqueous solution, and the droplet is assumed to enter a rapid growth regime, expressed by a "pure" water $\alpha_{rapid} = 0.042$ [*Pruppacher and Klett*, 1997]. Published values of α_{rapid} varies considerably, ranging between 0.04 to 1. *Fung et al.* [1987] were able to fit α_{rapid} with a value close to unity from condensational growth measurements on a pure NaCl droplet using Mie resonance spectroscopy. The value of α_{rapid} is closer to 0.01 for aged atmospheric droplets [*Pruppacher and Klett*, 1997] and maybe as low as 0.04 for pure water [*Shaw and Lamb*, 1999; *Li et al.*, 2001]. For this study, we used 0.042 as it is widely accepted for atmospheric droplets in the atmospheric community [*Pruppacher and Klett*, 1997].

As the chemical composition of FFCs and their accommodation properties are not known, we consider values for α_{slow} ranging from 10^{-5} to 10^{-3}. The lower end value of α_{slow} is consistent with values estimated by *Chuang* [2003]. The "critical" film thickness (film

thickness required for the film to break) is assumed to equal a monolayer coverage of cetyl alcohol molecules (~10^{-10} m) [*Feingold and Chuang*, 2002; *Nenes et al.*, 2002a] and represents the maximum effect a film can exert on the growth of a droplet. The film thickness is related to the volume of FFCs in a particle, which in turn is directly related to ε_o and $D_{p,dry}$. Figure 4 presents the threshold diameter required for the film on a droplet to break as a function of its $D_{p,dry}$ and ε_o. Although it may be possible for a film to break before reaching its "critical" film thickness, this is not explored; the current simulations however can be related to films that break at any "critical" film thickness.

4. Simulation Results

4.1 GCCN maximum size reductions. To systematically explore the influence of FFCs on GCCN growth, we examine $r_{\max}$, the ratio of the maximum in-cloud diameter of GCCN if they contain FFCs, $D_p^{\max}(\varepsilon_o)$, over the maximum diameter they attain in the absence of FFCs, $D_p^{\max}(\varepsilon_o = 0)$:

$$r_{\max} = \frac{D_p^{\max}(\varepsilon_o)}{D_p^{\max}(\varepsilon_o = 0)} \tag{16}$$

The lower the value of $r_{\max}$, the more effective FFCs are in inhibiting the condensational growth of GCCN. Figure 5 presents $r_{\max}$ as a function of $D_{p,dry}$ for supersaturation trajectories derived from ASTEX-1 for pristine aerosol conditions. $r_{\max}$ is primarily affected by α_{slow}; when α_{slow} is equal to 10^{-3}, $r_{\max}$ ranges between 0.7 and 1.0 but when α_{slow} is equal to 10^{-5}, $r_{\max}$ is between 0.1 and 0.4. Similar behavior is seen in both ASTEX-1 and ASTEX-2 trajectories for pristine and polluted conditions (not shown). In addition to α_{slow}, $r_{\max}$ also

depends on $D_{p,dry}$, ε_o, and ε_s. Figure 6 (which is the same as Figure 5, but for $\alpha_{slow} = 10^{-5}$) is used to explain the effect of each parameter on $r_{\max}$ through three examples. "Case 1" represents $r_{\max}$ as a function of $D_{p,dry}$, "Case 2" presents $r_{\max}$ as a function of ε_o, and "Case 3" shows $r_{\max}$ as a function of ε_s.

"Case 1" corresponds to ε_o = 5% and ε_s = 50%. For small $D_{p,dry}$, $r_{\max}$ decreases with increasing $D_{p,dry}$ until it reaches a minimum value. For large values of $D_{p,dry}$, $r_{\max}$ curves converge to a common curve. Typically, GCCN with $D_{p,dry} \geq$ 15 μm approach this limit in all the cloud conditions considered in this study. This asymptote depends on the value of α_{slow} (Figure 5). The behavior of $r_{\max}$ can be rationalized if it is related to the GCCN dry size:

$$r_{\max} = \frac{D_p^{\max}(\varepsilon_o)}{D_p^{\max}(\varepsilon_o = 0)} \approx \frac{D_{p,dry} + \Delta D_{p,cg}^{\max}}{D_{p,dry} + \Delta D_{p,cg}^{\max}(\varepsilon_o = 0)} \tag{17}$$

$\Delta D_{p,cg}^{\max}$ and $\Delta D_{p,cg}^{\max}(\varepsilon_o = 0)$ represent the maximum average condensational growth when FFCs are present and absent, respectively. GCCN with small $D_{p,dry}$ grow enough in most trajectories to break their films and experience significant growth with α_{rapid}. Under these conditions, $\Delta D_{p,cg}^{\max} \approx \Delta D_{p,cg}^{\max}(\varepsilon_o = 0)$ allowing $r_{\max}$ to approach unity. As $D_{p,dry}$ increases, the amount of organic material also increases and fewer GCCN experience film rupture. Thus, there is less condensational growth and $\Delta D_{p,cg}^{\max}$ is smaller than $\Delta D_{p,cg}^{\max}(\varepsilon_o = 0)$, forcing $r_{\max}$ to decrease. At a characteristic dry diameter, $D_{p,dry}^*$, the films in all trajectories do not rupture; thus, the condensational growth (and $r_{\max}$) reaches a minimum value. For $D_{p,dry}$ >

$D^*_{p,dry}$, $\Delta D^{\max}_{p,cg}$ does not change much and $r_{\max}$ varies monotonically with $D_{p,dry}$. It is important to examine the values of $D^*_{p,dry}$ to assess which range of GCCN sizes display the strongest sensitivity to the presence of FFCs. From Figure 5 and 6, we consistently see that $D^*_{p,dry}$ ranges between 5 and 12 μm, which is the size range where most GCCN are likely to exist [*Exton et al.*, 1986]. This means that GCCN are more likely to exhibit the maximum sensitivity to the presence of FFCs.

Since all trajectories in the cloud do not exhibit the same supersaturation history, not all GCCN will concurrently experience bursting of their films. The relative proportion of "rapidly" to "slowly" growing GCCN will thus depend, in addition to the parcel supersaturation, on ε_o. "Case 2", represented by three simulation points on Figure 6, illustrates this effect. When ε_o is less than 0.2%, $r_{\max}$ approaches unity. As ε_o increases to 0.5%, $r_{\max}$ decreases to approximately 0.6. When ε_o is about 1%, $r_{\max}$ is 0.25; additionally increasing ε_o does not further decrease $r_{\max}$. Equation 17 can be used to explain this dependence. For small values of ε_o, many droplets experience rapid condensational growth as their films rupture. This translates to $\Delta D^{\max}_{p,cg} \approx \Delta D^{\max}_{p,cg}(\varepsilon_o = 0)$, or $r_{\max}$ approximately unity. As ε_o increases, less and less of the GCCN can grow enough to break their films; at a characteristic ε^*_o, none of the GCCN can break their films and $\Delta D^{\max}_{p,cg}$ becomes minimum for the GCCN in all trajectories. Thus, for $\varepsilon_o > \varepsilon^*_o$ (in our case $\varepsilon^*_o \sim 1\%$), $r_{\max}$ remains constant.

The hygroscopicity of GCCN is determined by the amount of soluble material present. The more hygroscopic GCCN are, the larger the driving force for condensational growth (Equation 8); furthermore, their equilibrium size with ambient RH is larger below

cloud [*Seinfeld and Pandis*, 1998]. Both factors contribute to a larger wet size of the GCCN in-cloud when compared to less hygroscopic CCN with the same dry diameter; thus increasing the hygroscopicity would facilitate film rupture. "Case 3" examines the effect of ε_s on $r_{\max}$. When the ε_s equals 25%, $r_{\max}$ is 0.35. When ε_s equals 50% and 75%, $r_{\max}$ is 0.7 and 0.85, respectively. The soluble fraction effect is more pronounced at small $D_{p,dry}$, as less growth (compared to larger $D_{p,dry}$) is necessary to rupture the films.

4.2 GCCN sizes. The analysis in Section 4.1 was an attempt to rationalize and parameterize the effect of FFCs on GCCN growth. In terms of the microphysical evolution of a cloud, what is ultimately important is the absolute size of the GCCN in the cloud. As proposed by *Feingold et al*. [1999], we consider GCCN as effective collector drops if their size in-cloud is 40 μm or greater.

Figure 8 presents the average growth of a 5 μm GCCN under pristine conditions for different values of α_{slow} and with ε_o equal to 0.2% (Figure 8a), and 0.5% (Figure 8b). In Figure 8, FFC-free GCCN can grow to 50 μm (e.g., it can act as a collector drop). In Figure 8a, for α_{slow} equal to 10^{-3} and 10^{-4}, the reduction in size is minimal. This is expected; under these conditions of ε_o and α_{slow}, $r_{\max}$ approaches 1 (Figure 6). For α_{slow} equal to 10^{-5}, the GCCN growth is inhibited and the maximum size reached is below the threshold of 40 μm. Increasing ε_o (Figure 8b) results in a more pronounced reduction in GCCN size; in contrast to Figure 8a, a reduction of about 10 μm (which is significant, given that the GCCN is now about the 40 μm size threshold) is seen throughout the cloud for α_{slow} equal to 10^{-4}. Almost complete inhibition in growth is seen for $\alpha_{slow} = 10^{-5}$; the GCCN only grows to a size of 10

μm, and is effectively indistinguishable from any other cloud droplet. Increasing ε_o to 1% further decreases the GCCN size when α_{slow} is 10^{-4}, and as expected, almost complete inhibition in growth is seen when α_{slow} is equal to 10^{-5} (not shown).

Figure 9 presents simulations for a 5 μm GCCN under polluted conditions. Under these conditions, the FFC-free GCCN can still exceed the 40 μm size threshold and act as an effective collector drop. If a small amount of FFC is present (ε_o = 0.2%), negligible reductions in size are seen for α_{slow} between 10^{-3} and 10^{-4} (Figure 9a). Strong reductions in size, however, are seen if α_{slow} = 10^{-5}. Increasing ε_o to 0.5% (Figure 9b) significantly reduces the GCCN size for α_{slow} = 10^{-4}; almost complete inhibition in growth is seen for α_{slow} = 10^{-5}. By comparing Figures 8 and 9, a striking observation arises: the ability of a GCCN to grow is strongly dependent on ε_o (e.g. film thickness) and α_{slow}, but not on the cloud supersaturation characteristics.

It is important to assess whether the conclusions from Figures 8 and 9 apply to GCCN of larger $D_{p,dry}$. Figure 10 presents growth curves for a 10 μm GCCN for both pristine and polluted cloud conditions. In the absence of FFCs (Figure 10a), the 10 μm GCCN grows to about 60 μm in diameter and can act as a collector drop. When the GCCN contains 0.2% FFCs, the growth is reduced somewhat when α_{slow} ranges between 10^{-4} and10^{-3}, but not enough to prevent the GCCN from growing past 40 μm (Figure 10a). Nevertheless, for α_{slow} equal 10^{-5}, the GCCN is prevented from becoming a collector drop; in fact, both pristine and polluted simulations overlap and display the same growth behavior. Increasing the FFC mass fraction to 1% exemplifies the growth inhibition for both polluted and pristine conditions

(Figure 10b). In Figure 10b, significant reductions in size are seen even for α_{slow} equal to 10^{-4}.

Up to this point, we have examined the growth of individual GCCN within the cloud trajectory ensemble. In reality, there is a size distribution of GCCN present within a cloud; it is therefore instructive to extend our analysis to a polydisperse GCCN population using *Whitby* [1978] distributions within a size range of 1 to 25 μm. Figure 11 shows the fraction of this GCCN population whose size exceeds 40 μm as a function of ε_o. The results were obtained from ASTEX-1 trajectories under pristine conditions. In the absence of FFCs (e.g. ε_o = 0), about 30% of the GCCN become larger than 40 μm, thus potentially acting as collector drops. When FFCs are included, the fraction of GCCN whose size reaches threshold significantly decreases even if a small amount of FFCs are present. For example, when ε_o is about 2%, less than 10% of the GCCN within the population exceed the 40 μm threshold.

5. Summary and Conclusions

Our analysis indicates that the presence of FFCs in GCCN can influence the microphysical evolution of clouds through this previously unexplored mechanism. FFCs decrease the rate of mass transfer of water vapor to/from the GCCN expressed by a reduction in the accommodation coefficient, α_{slow}. This study shows that for α_{slow} ranging from 10^{-3} to 10^{-5}, GCCN within the trajectory sets experienced a 30%-90% reduction in size when compared to GCCN growing with a "pure water" accommodation coefficient of 0.042. For GCCN with dry diameters greater than 15 μm, α_{slow} is the primary parameter affecting the droplet size; not so with GCCN with dry diameters less than 15 μm, which were found to be dependent on the initial dry diameter as well as the FFC content. Whether or not the film

ruptures is a deciding factor for the droplet size. Lowering the FFC mass fraction and increasing the hygroscopicity of the GCCN tend to facilitate the rupture of films.

The absolute wet diameter of GCCN in the cloud simulations is important to assess its effectiveness as a collector drop; in this study, we used a threshold diameter of 40 μm to classify the GCCN as a collector drop. This study shows that the conditions to exceed the threshold is a weak function of the cloud supersaturation history (i.e., whether it corresponded to pristine or polluted aerosol conditions); this opens the possibility of parameterizing this mechanism. The results also indicate that very low mass fractions of organic film forming compounds (FFCs) are needed to render a GCCN an inefficient collector drop. Under certain conditions, FFC mass fractions as low as 0.5%, delayed the growth of a 5 μm GCCN to such an extent that its final size was indistinguishable from a typical cloud droplet (~10 μm). It is quite likely that the threshold diameter for becoming a collector drop would vary from cloud to cloud. This uncertainty does not have a significant impact on our conclusions, as the effect of FFCs on growth is potentially very strong.

In addition to affecting the accommodation properties, FFCs, being surfactants may, together with the water-soluble organics, decrease droplet surface tension. The latter has been shown to have an important effect on droplet number (e.g., *Facchini et al.*, 1999; *Nenes et al.*, 2002a). Such effects are neglected here, but are not expected to have a significant impact on our results; GCCN already have very low critical supersaturations, S_c, (~ 0.01%), so an additional decrease in S_c is not expected to appreciably affect growth. FFCs however may be partially soluble, so they can affect droplet growth by introducing another kinetic limitation, being the finite dissolution time (e.g., *Shantz et al.*, 2003). The significance of this mechanism remains to be explored. The additional hygroscopicity from the soluble fraction,

although not explicitly considered here in the model, would not exceed that of $(NH_4)_2SO_4$ and thus lie within the range explored. It is also possible that the hydrophobic films may undergo oxidative reactions [*Eliason et al.*, 2004] and be converted to water-soluble compounds. The timescale required for air masses to be aged (oxidized) is much larger than the lifetime of freshly emitted marine GCCN which may be on the order of hours [*Gong et al.*, 2002]. Thus, it is likely that the films may retain their hydrophobic state over the course of the GCCN lifetime. As both biogenic and anthropogenic sources emit large amounts of hydrophobic compounds that potentially can act as FFCs, it is likely that local sources of FFC are ubiquitous throughout the atmosphere and responsible for the accommodation properties of the CCN.

The most striking result of this study is that small quantities of FFCs, if present in GCCN, may have the potential to change a cloud from a precipitating to a non-precipitating state. Together with the synergistic effect of black carbon [*Nenes et al.*, 2002], GCCN may be influencing the microphysical evolution of clouds to a lesser extent than previously thought. Therefore, understanding the frequency of occurrence and accommodation properties of FFCs is required to advance the understanding and modeling capability of the hydrological cycle.

Acknowledgements. This work was supported by NASA Headquarters under the Earth System Science Fellowship Grant NGT5-30506. We would also like to thank Bjorn Stevens and Graham Feingold for providing the trajectories from the LES simulations.

References

Albrecht, B.A., Aerosols, cloud microphysics, and fractional cloudiness, *Science*, **245**, 1227-1230, 1989.

Albrecht, B. A., C. S. Bretherton, D. Johnson, W. H. Scubert, and A. S. Frisch, The Atlantic Stratocumulus Transition Experiment: ASTEX, *Bull. Am. Meteorol. Soc.*, **76**, 889– 904, 1995.

Chuang, P. Y., Measurement of the timescale of hygroscopic growth for atmospheric aerosols, *J. Geophys. Res.*, **108** (D9), 4282, doi:10.1029/2002JD002757, 2003.

Conant, W., A. Nenes, and J. Seinfeld, Black carbon radiative effect on cloud microphysics and implications for the aerosol indirect effect: 1. Extended Köhler theory, *J. Geophys. Res.*, **107** (D21), 4604, doi: 10.1029/2002JD002094, 2002.

Cooper, W. A., R. T. Bruintjes, and G. K. Mather, Calculations pertaining to hygroscopic seeding with flares, *J. Appl. Meteor.*, **36**, 1449-1469, 1997

Cruz, C. N., and S. N. Pandis, The effect of organic coatings on the cloud condensation nuclei activation of inorganic atmospheric aerosol, *J. Geophys. Res.*, **103** (D11), 13111-13123, 1998.

Eliason T.L., J.B Gilman J.B. and V. Vaida, Oxidation of organic films relevant to atmospheric aerosols, *Atmos.Environ.*, **38**, 1367-1378, 2004

Exton, H. J., J. Latham, P. M. Park, M. H. Smith, and R. R. Allan, *The production and dispersal of maritime aerosol. Oceanic Whitecaps and Their Role in Air–Sea Exchange Processes*, E. C. Monahan and G. Mac Niocaill, Eds., Oceanic Sciences Library, D. Reidel, 175–193, 1986

Facchini, M. C., M. Mircea, S. Fuzzi, and R. Charlson, Cloud albedo enhancement by surface-active organic solutes in growing droplets, *Nature*, **401**, 257-259, 1999.

Feingold, G., and P. Chuang, Analysis of the influence of film-forming compounds on droplet growth: Implications for cloud microphysical processes and climate, *J. Atmos. Sci.*, **59**, 2006-2018, 2002.

Feingold, G., W. R. Cotton, S. M. Kreidenweiss, and J. T. Davis, The impact of giant cloud condensation nuclei on drizzle formation in stratocumulus: implication for cloud radiative properties, *J. Atmos. Sci.*, **56**, 4100-4117, 1999.

Gong S.L., L.A. Barrie, and M. Lazare, Canadian Aerosol Module (CAM): A size-segregated simulation of atmospheric aerosol processes for climate and air quality models - 2. Global sea-salt aerosol and its budgets, *J.Geophys.Res.*, **107** (D24), Art. No. 4779, 2002

Gill, P. S., T. E. Graedel, and C. J. Weschler, Organic films on atmospheric aerosol particle, fog droplets, cloud droplets, raindrops, and snowflakes, *Rev. Geophys. Space Phys.*, **21**, 903-920, 1983.

Haywood, J., O. Boucher, Estimates of the direct and indirect radiative forcing due to tropospheric aerosols: A review, *Reviews of Geophysics*, **38**, 513–543, 2000.

Hindmarsh, A. C., *ODEPACK: a systematized collection of ODE solvers*, Scientific Computing, edited by R. S. Stepleman, pp. 55-64, North-Holland Publishing Company, New York, 1983.

Johnson, D. B., The role of giant and ultragiant aerosol particles in warm rain initiation, *J. Atmos. Sci.*, **39**, 448-460, 1982

Kulmala, M., A. Laaksonen, P. Korhonen, T. Vesala, T. Ahonen, and J. Barret, The effect of atmospheric nitric acid vapor on cloud condensation nucleus activation, *J. Geophys. Res.*, **98** (D12), 22949-22958, 1993.

Lelieveld, J., P. Crutzen, V. Ramanathan, M. Andreae, C. Brenninkmeijer, T. Campos, G. Cass, R. Dickerson, H. Fischer, J. de Gouw, A. Hansel, A. Jefferson, D. Kley, A. de Laat, S. Lal, M. Lawrence, J. Lobert, O. Mayol-Bracero, A. Mitra, T. Novakov, S. Oltmans, K. Prather, T. Reiner, H. Rodhe, H. Scheeren, D. Sikka, J. Williams, The Indian Ocean Experiment: Widespread air pollution from South and Southeast Asia, *Science*, **291**, 1031-1036, 2001.

Nenes, A., S. Ghan, H. Abdul-Razzak, P. Y. Chuang, J. H. Seinfeld, Kinetic limitations on cloud droplet formation and impact on cloud albedo, *Tellus*, **53B**, 133-149, 2001.

Nenes, A., R. J. Charlson, M. C. Facchini, M. Kulmala, A. Laaksonen, J. H. Seinfeld, Can chemical effects on cloud droplet number rival the first indirect effect?, *Geophys. Res. Lett.*, **29** (17), Art. No. 1848, 2002a.

Nenes, A., W. C. Conant, and J. H. Seinfeld, Black Carbon radiative heating effects on cloud microphysics and implications for the aerosol indirect effect: 2. Cloud Microphysics, *J. Geophys. Res.*, **107**, doi: 10.1029/2002JD002,101, 2002b.

Pruppacher, H., and J. Klett, *Microphysics of Clouds and Precipitation*, 2nd ed., Kluwer, Dordrecht, 1997.

Rosenfeld, D., L. R. Khain, M. Pinsky, The role of sea spray in cleansing air pollution over ocean via cloud processes, *Science*, **297**, 1667-1670, 2002.

Rudich, Y., O. Khersonsky, D. Rosenfeld, Treating clouds with a grain of salt, *Geophys. Res. Lett.*, **29** (22), 2060, doi:10.1029/2002GL016055, 2002.

Saxena, P., L. M. Hildermann, P. H. McMurry and J. H. Seinfeld, Organics alter the hygroscopic behavior of atmospheric particles, *J. Geophys. Res.*, **100**, 18,755-18,770, 1995.

Seinfeld, J. H., S. N. Pandis, *Atmospheric Chemistry and Physics: From Air Pollution to Climate Change*, John Wiley, New York, 1998.

Shantz, N. C., W. R. Leaitch, P. F. Caffrey, Effect of organics of low solubility on the growth rate of cloud droplets, *J. Geophys. Res.*, **108** (D5), 4168, doi:10.1029/2002JD002540, 2003.

Shulman, M., M. Jacobson, R. Charlson, R. Synovec, and T. Young, Dissolution behavior and surface tension effects of organic compounds in nucleating cloud droplets, *Geophys. Res. Lett.*, **23**, 277-280, 1996.

Shulman, M. L., R. J. Charlson and E. J. Davis, The effects of atmospheric organics on aqueous droplet evaporation, *J. Aerosol Sci.*, **28**, 737-752, 1997.

Stevens, B., G. Feingold, W. Cotton, and R. Walco, Elements of the microphysical structure of numerically simulated nonprecipitating stratocumulus, *J. Aerosol Sci.*, **53**, 980-1006, 1996.

Tervahattu H., K. Hartonen, V. M. Kerminen, K. Kupiainen, P. Aarnio, T. Koskentalo, A.F. Tuck, V. Vaida, New evidence of an organic layer on marine aerosols, *J.Geophys.Res.*, **107**, Art. No. 4053, 2002a

Tervahattu H., J. Juhanoja, K. Kupiainen, Identification of an organic coating on marine aerosol particles by TOF-SIMS, *J.Geophys.Res.*, **107**, Art. No. 4319, 2002b

Twomey, S., Minimum size of particle for nucleation in clouds, *J. Atmos. Sci.*, **34** (11), 1832-1835, 1977.

Tzivion, S., T. Reisin, and Z. Levin, Numerical simulation of hygroscopic seeding in a convective cloud, *J. Appl. Meteor.*, **33**, 252-267, 1994

Whitby, K.T., The physical characteristics of sulfur aerosols, *Atmos. Environ.*, **12**, 135-159, 1978.

Tables

Table 1. Aerosol distribution parameters ($D_{g,i}, \sigma_i, N_i$) (*Whitby*,[1978]) $D_{g,i}$ represents the average diameter (μm), N_i is the number concentration (cm^{-3}), and σ_i is the geometric standard deviation for each mode.

Aerosol Type	Nuclei Mode			Accumulation Mode			Coarse Mode		
	$D_{g,1}$	σ_1	N_1	$D_{g,2}$	σ_2	N_2	$D_{g,3}$	σ_3	N_3
Marine	0.010	1.6	340	0.070	2.0	60	0.62	2.7	3.1
Urban	0.014	1.8	106000	0.054	2.16	32000	0.86	2.21	5.4

Figure Captions

FIGURE 1. Overview of the methodology used in calculating the growth of GCCN using the LES-derived Lagrangian trajectories.

FIGURE 2. Vertical profiles of updraft velocity characteristics for stratocumulus cloud (a) ASTEX-1 and (b) ASTEX-2.

FIGURE 3. Illustration of the "Breaking film" model adapted in this study. Film-covered droplets experience slow condensational growth. When the threshold size required to break the film is reached, the droplet enters a rapid growth phase.

FIGURE 4. The diameter required for a growing droplet to break its organic film as a function of ε_o and $D_{p,dry}$.

FIGURE 5. $r_{\max}$ as a function of $D_{p,dry}$, for a variety of α_{slow} (10^{-3}, 10^{-4}, 10^{-5}), ε_s (25%, 50%, 75%) and ε_o (0.2%, 0.5%, 1%, 5%). The simulations are for the ASTEX-1 cloud with pristine aerosol conditions.

FIGURE 6. Same as Figure 5, except that simulations are for one value of α_{slow} (10^{-5}).

FIGURE 7. $r_{\max}$ as a function of ε_o with a constant ε_s = 25%, for a variety of $D_{p,dry}$ (2.5 μm, 5 μm, 10 μm) and α_{slow} (10^{-3}, 10^{-4}, 10^{-5}). The simulations are for the ASTEX-1 cloud for pristine aerosol conditions.

FIGURE 8. Average growth of a 5 μm GCCN , for the ASTEX-1 cloud with pristine aerosols conditions. The ε_s is constant at 25%. When FFCs are absent (e.g. ε_o = 0%), $\alpha_{slow} = \alpha_{rapid} = 0.042$. **a)** ε_o = 0.2%. **b)** ε_o = 0.5%.

FIGURE 9. Same as Figure 8, except that simulations are for the ASTEX-1 cloud with polluted aerosols conditions. **a)** ε_o = 0.2%. **b)** ε_o = 0.5%.

FIGURE 10. Same as Figure 8, except that simulations present a 10 μm GCCN for both pristine (white) and polluted (black) conditions. **a)** ε_o = 0.2%. **b)** ε_o = 1%.

FIGURE 11. Fraction of GCCN that exceed the 40 μm size threshold as a function of ε_o. The simulations correspond to the ASTEX-1 cloud with pristine aerosol conditions.

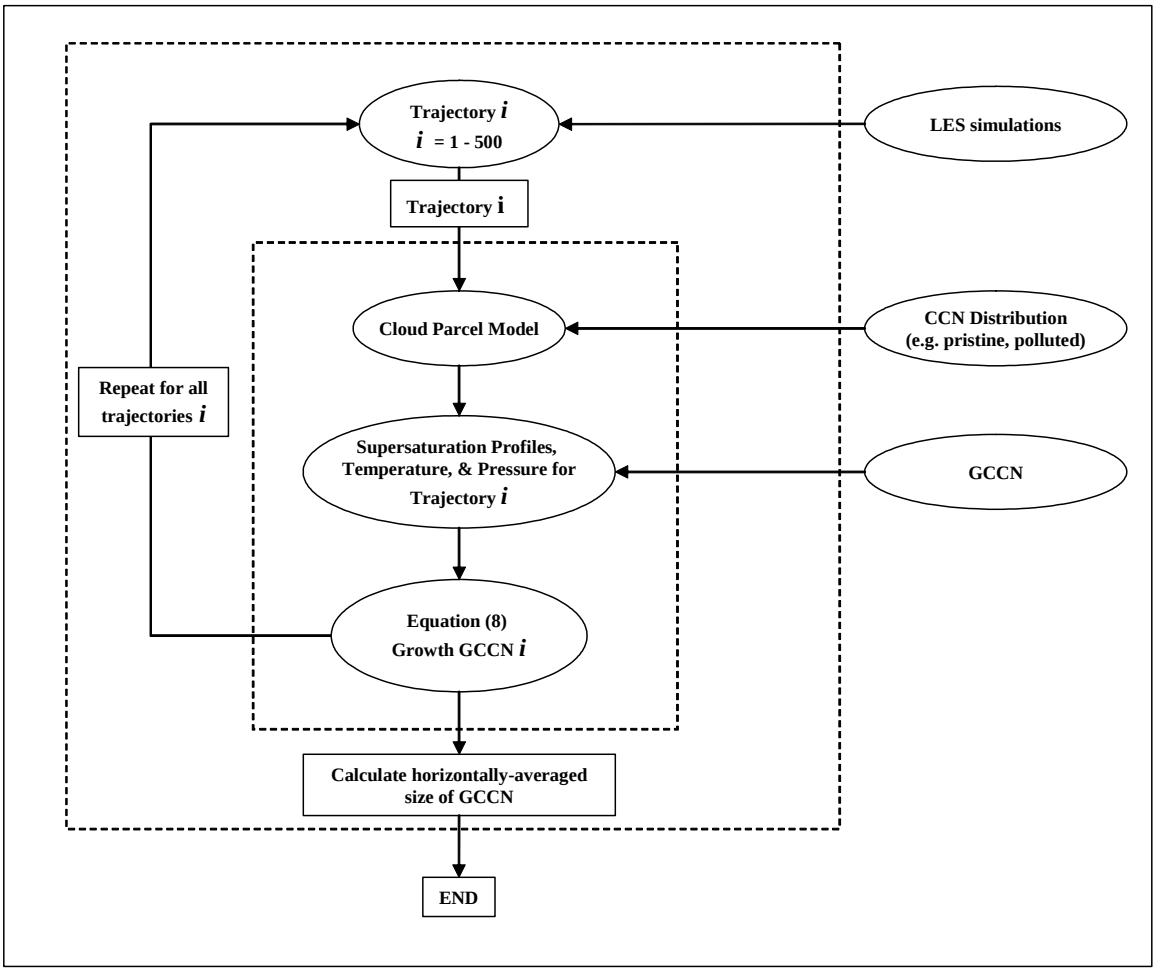
Trajectory i
i = 1 - 500
LES simulations
Trajectory i
Cloud Parcel Model
CCN Distribution
(e.g. pristine, polluted)
Repeat for all
trajectories i
Supersaturation Profiles,
Temperature, & Pressure for
Trajectory i
GCCN
Equation (8)
Growth GCCN i
Calculate horizontally-averaged
size of GCCN
END

FIGURE 1.

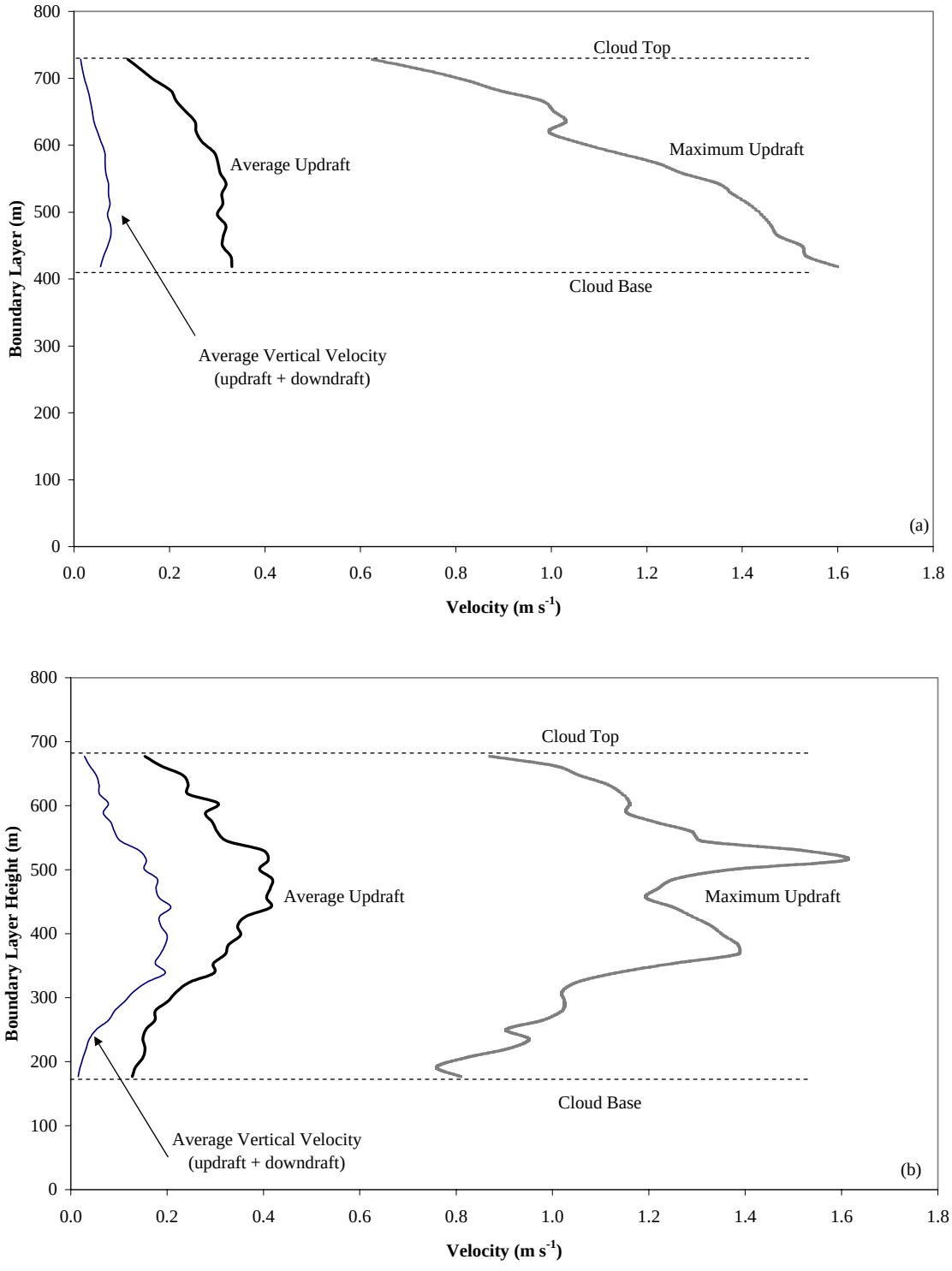
Cloud Top
Maximum Updraft
Average Updraft
Cloud Base
Average Vertical Velocity
(updraft + downdraft)
Boundary Layer (m)
Velocity (m s-1)
(a)
Cloud Top
Average Updraft
Maximum Updraft
Cloud Base
Average Vertical Velocity
(updraft + downdraft)
Boundary Layer Height (m)
Velocity (m s-1)
(b)

FIGURE 2.

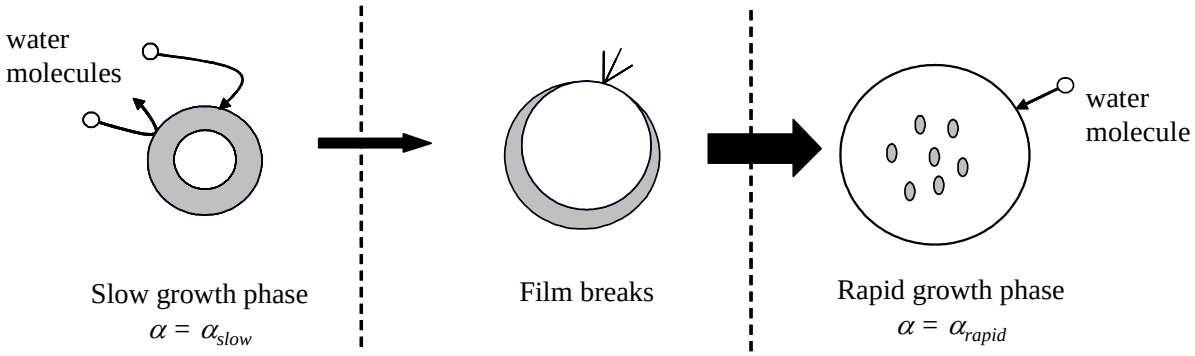
water
molecules
Slow growth phase
$\alpha = \alpha_{slow}$
Film breaks
water
molecule
Rapid growth phase
$\alpha = \alpha_{rapid}$

FIGURE 3.

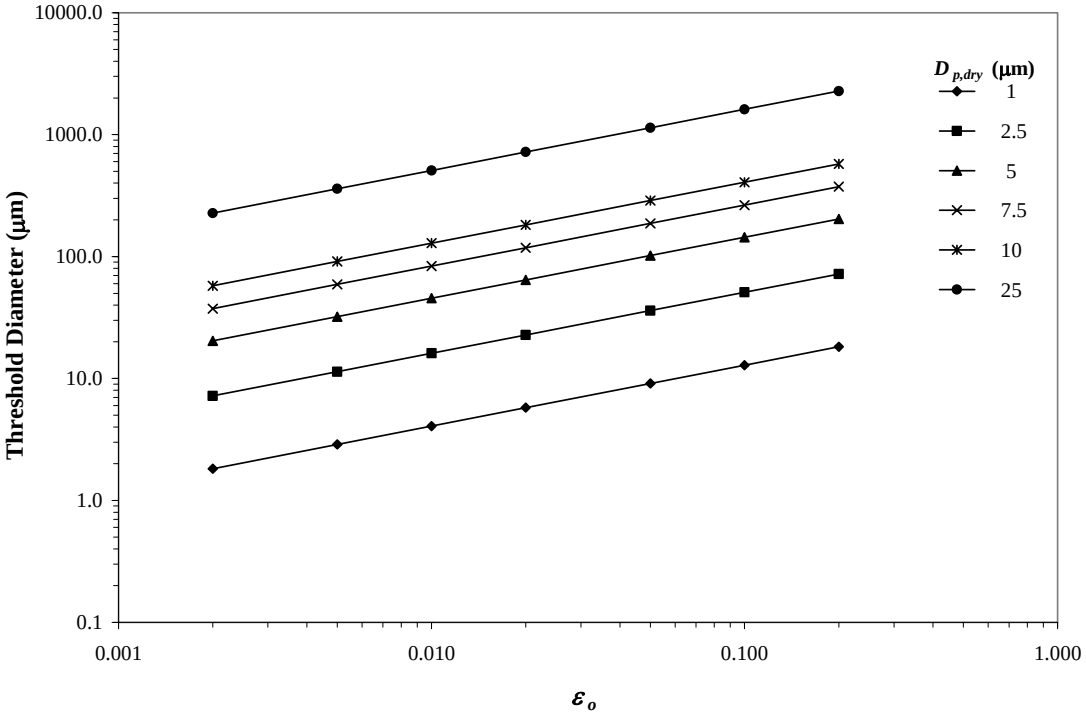
10000.0
1000.0
100.0
10.0
1.0
0.1
Threshold Diameter (μm)
0.001
0.010
0.100
1.000
ε_o
$D_{p,dry}$ (μm)
1
2.5
5
7.5
10
25

FIGURE 4.

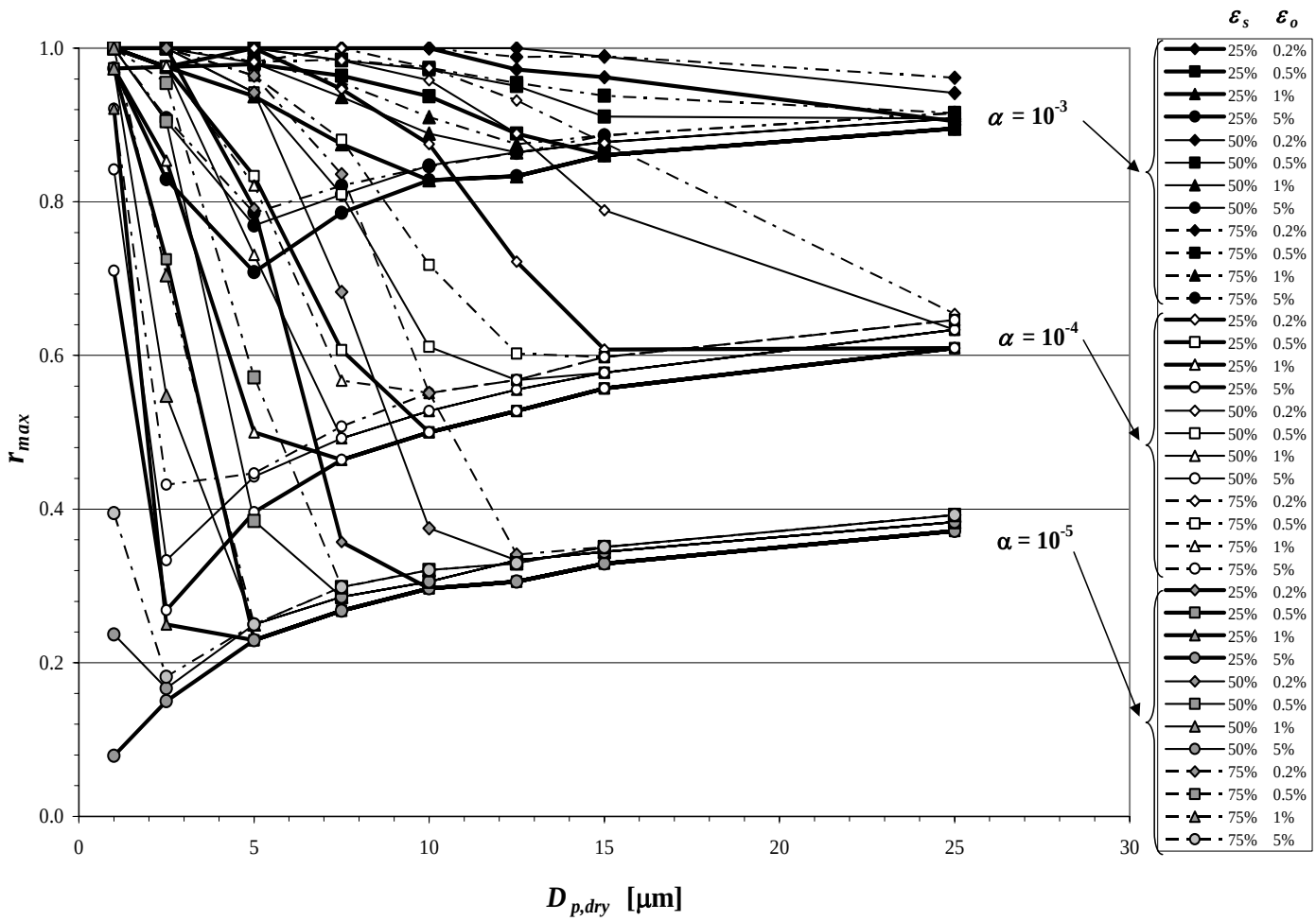
ε_s ε_o
25% 0.2%
25% 0.5%
25% 1%
25% 5%
50% 0.2%
50% 0.5%
50% 1%
50% 5%
75% 0.2%
75% 0.5%
75% 1%
75% 5%
$\alpha = 10^{-3}$
$\alpha = 10^{-4}$
$\alpha = 10^{-5}$
r_{max}
$D_{p,dry}$ [μm]
0.0
0.2
0.4
0.6
0.8
1.0
0
5
10
15
20
25
30

FIGURE 5.

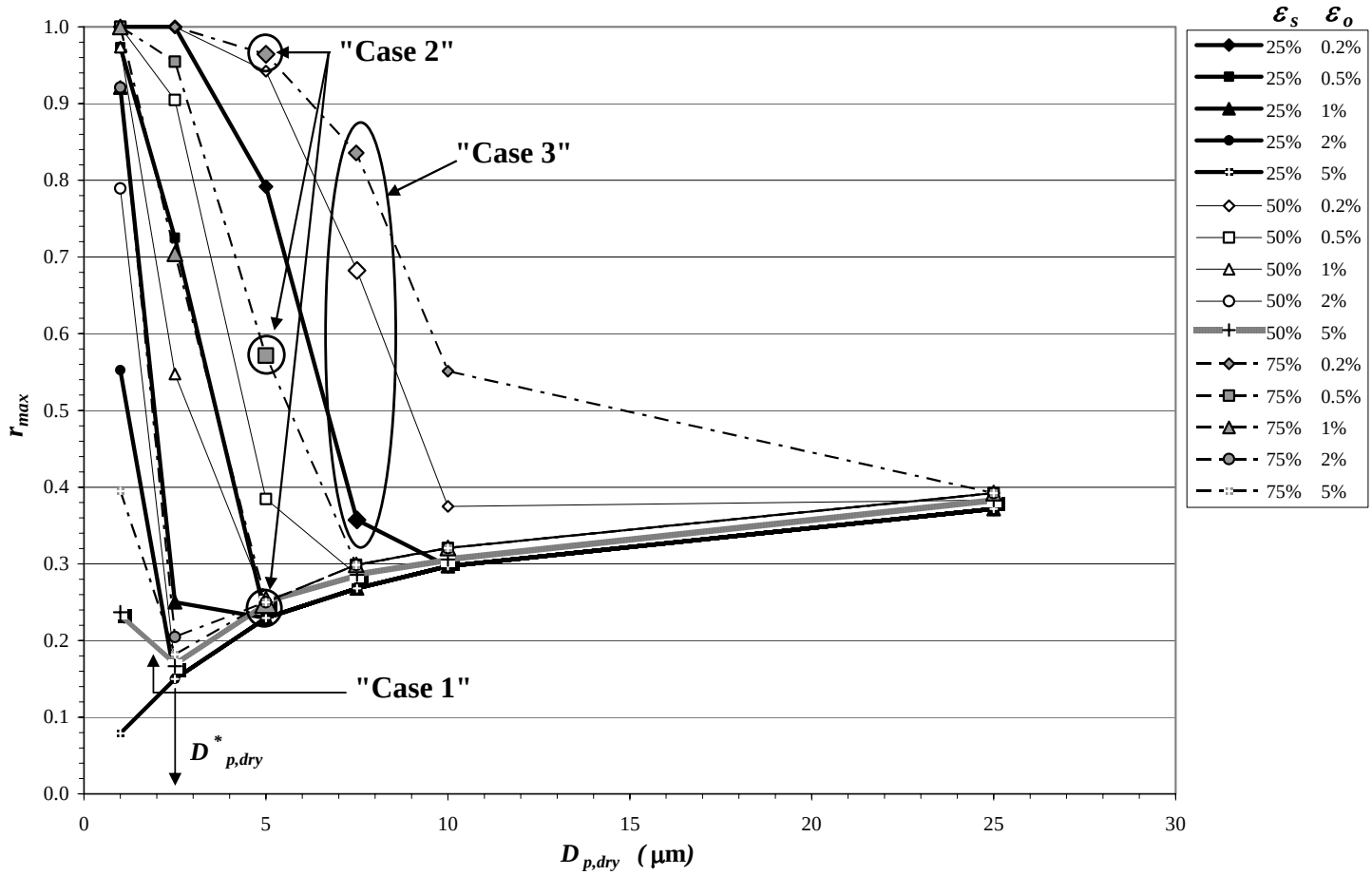
"Case 2"
"Case 3"
"Case 1"
$D^*_{p,dry}$
r_{max}
$D_{p,dry}$ (μm)
ε_s ε_o
25% 0.2%
25% 0.5%
25% 1%
25% 2%
25% 5%
50% 0.2%
50% 0.5%
50% 1%
50% 2%
50% 5%
75% 0.2%
75% 0.5%
75% 1%
75% 2%
75% 5%

FIGURE 6.

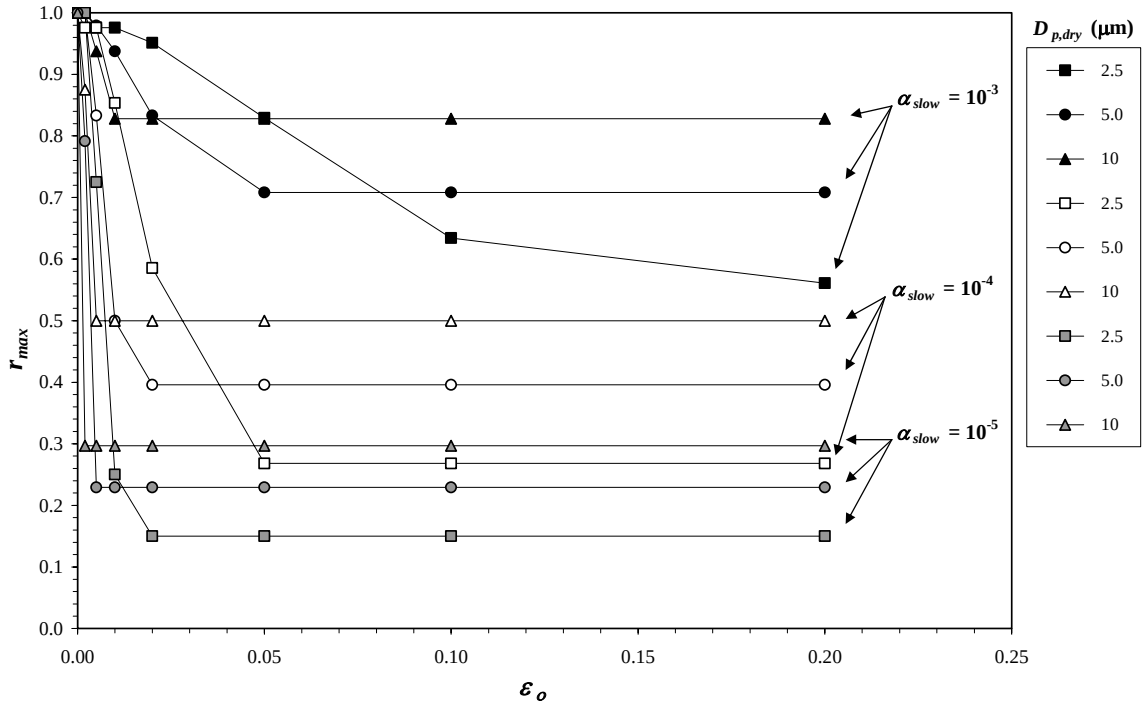
1.0
0.9
0.8
0.7
0.6
0.5
0.4
0.3
0.2
0.1
0.0
r_{max}
0.00
0.05
0.10
0.15
0.20
0.25
ε_o
$\alpha_{slow} = 10^{-3}$
$\alpha_{slow} = 10^{-4}$
$\alpha_{slow} = 10^{-5}$
$D_{p,dry}$ (μm)
2.5
5.0
10
2.5
5.0
10
2.5
5.0
10

FIGURE 7.

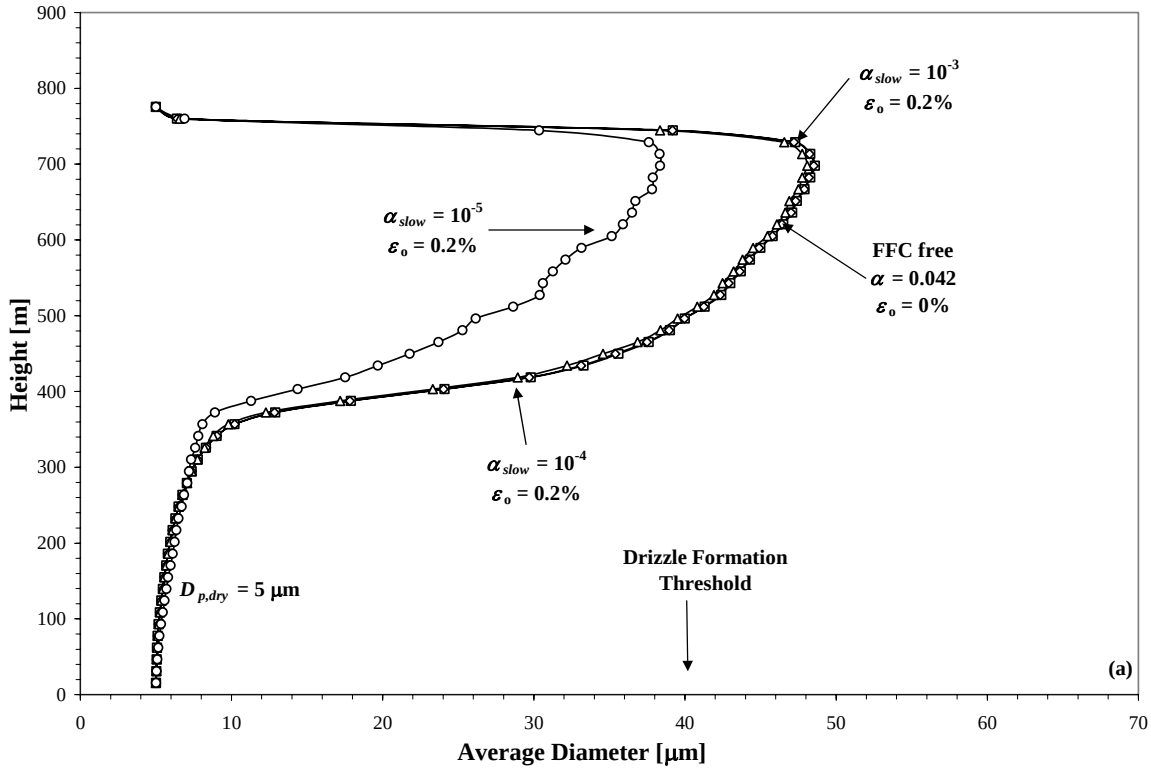
Height [m]
Average Diameter [μm]
$\alpha_{slow} = 10^{-3}$
$\varepsilon_o = 0.2\%$
$\alpha_{slow} = 10^{-5}$
$\varepsilon_o = 0.2\%$
FFC free
$\alpha = 0.042$
$\varepsilon_o = 0\%$
$\alpha_{slow} = 10^{-4}$
$\varepsilon_o = 0.2\%$
$D_{p,dry} = 5$ μm
Drizzle Formation Threshold
(a)

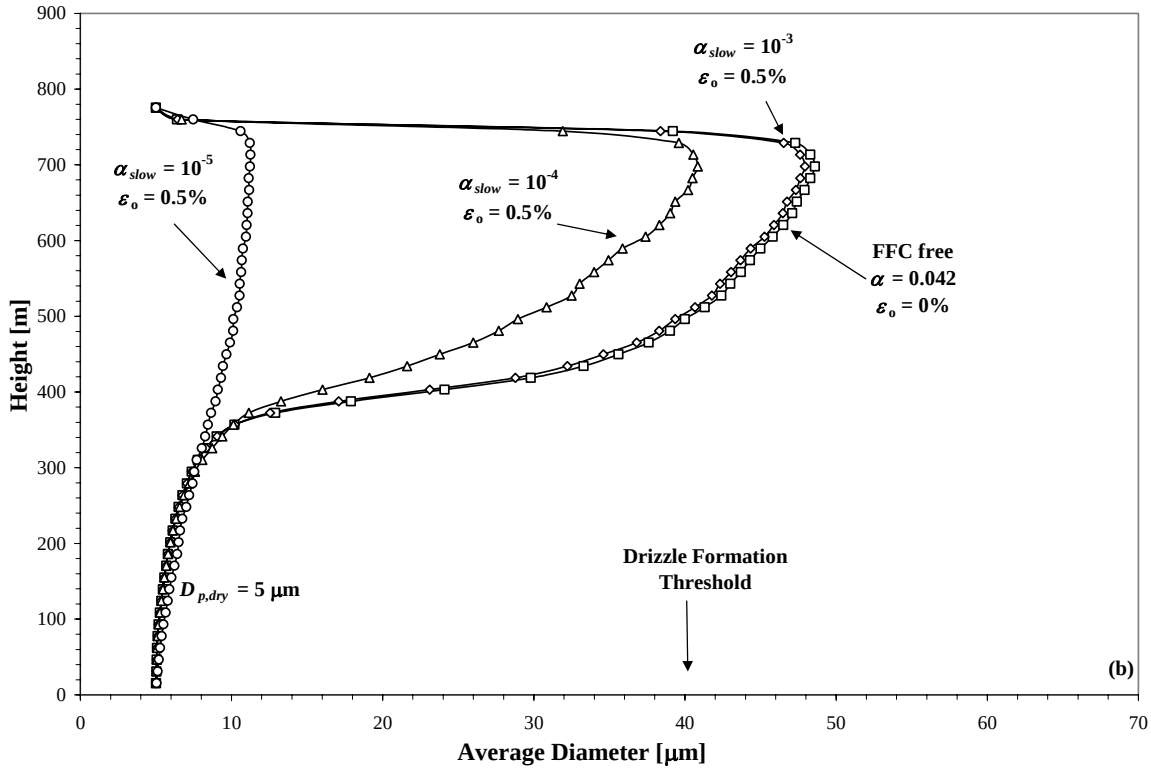
Height [m]
Average Diameter [μm]
$\alpha_{slow} = 10^{-3}$
$\varepsilon_o = 0.5\%$
$\alpha_{slow} = 10^{-5}$
$\varepsilon_o = 0.5\%$
$\alpha_{slow} = 10^{-4}$
$\varepsilon_o = 0.5\%$
FFC free
$\alpha = 0.042$
$\varepsilon_o = 0\%$
$D_{p,dry} = 5$ μm
Drizzle Formation Threshold
(b)

FIGURE 8.

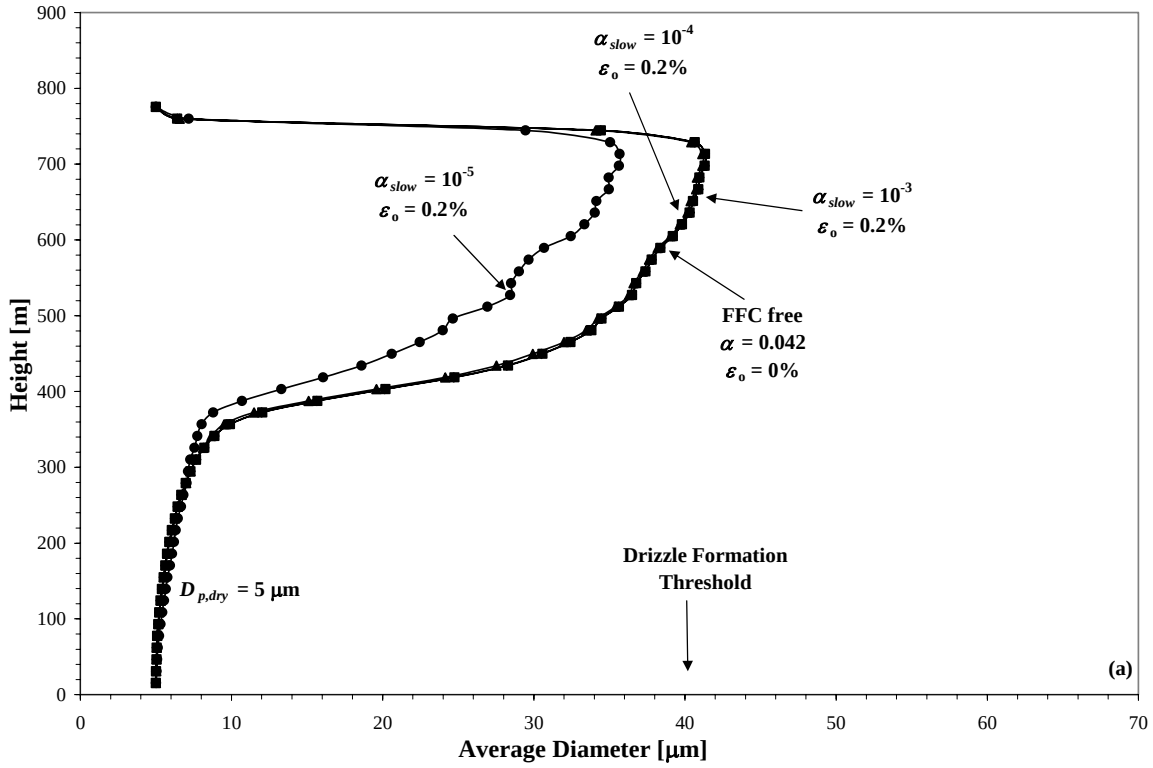
$\alpha_{slow} = 10^{-4}$
$\varepsilon_o = 0.2\%$
$\alpha_{slow} = 10^{-5}$
$\varepsilon_o = 0.2\%$
$\alpha_{slow} = 10^{-3}$
$\varepsilon_o = 0.2\%$
FFC free
$\alpha = 0.042$
$\varepsilon_o = 0\%$
Drizzle Formation Threshold
$D_{p,dry} = 5$ μm
(a)
Height [m]
Average Diameter [μm]
0
100
200
300
400
500
600
700
800
900
0
10
20
30
40
50
60
70

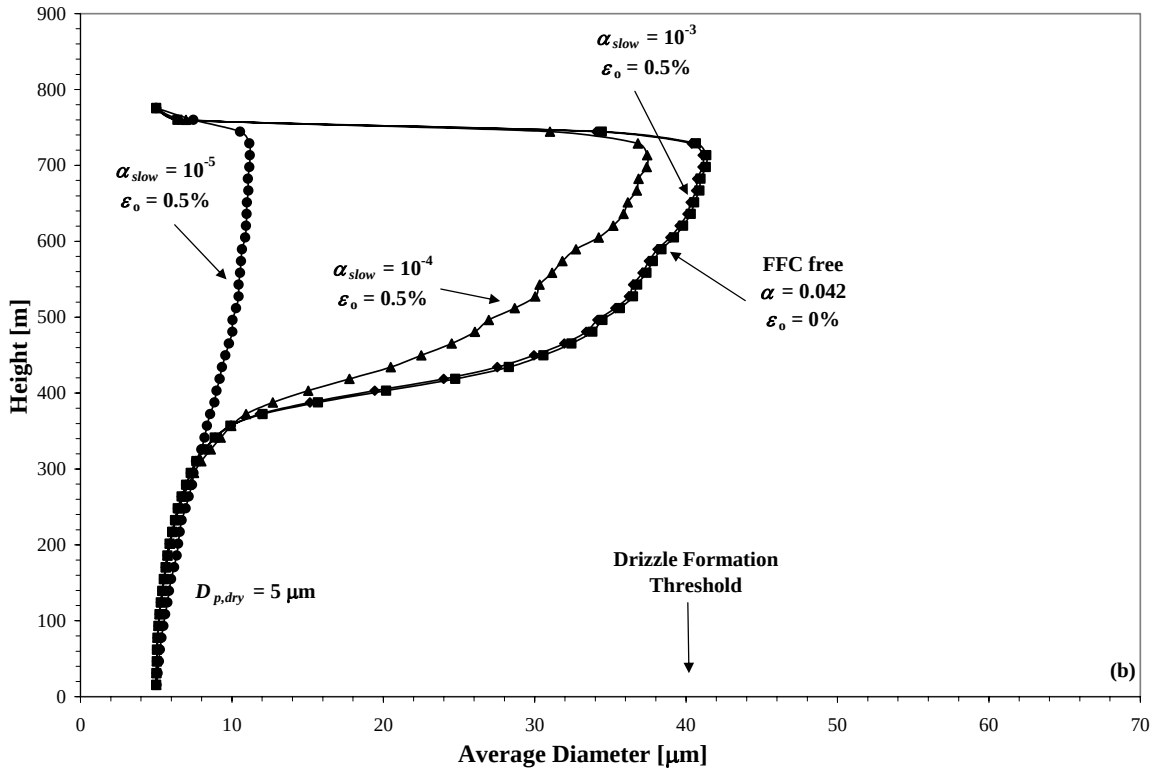
$\alpha_{slow} = 10^{-3}$
$\varepsilon_o = 0.5\%$
$\alpha_{slow} = 10^{-5}$
$\varepsilon_o = 0.5\%$
$\alpha_{slow} = 10^{-4}$
$\varepsilon_o = 0.5\%$
FFC free
$\alpha = 0.042$
$\varepsilon_o = 0\%$
Drizzle Formation Threshold
$D_{p,dry} = 5$ μm
(b)
Height [m]
Average Diameter [μm]
0
100
200
300
400
500
600
700
800
900
0
10
20
30
40
50
60
70

FIGURE 9.

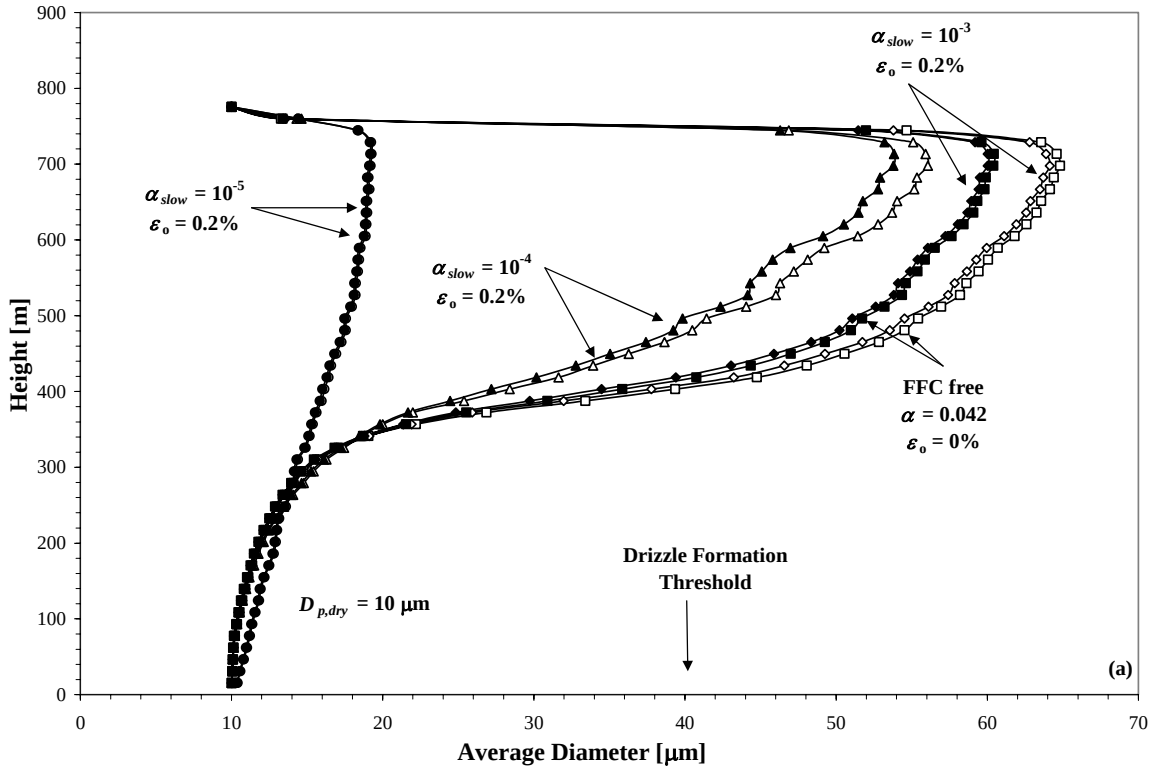
Height [m]
Average Diameter [μm]
α_{slow} = 10^{-3}
ε_o = 0.2%
α_{slow} = 10^{-5}
ε_o = 0.2%
α_{slow} = 10^{-4}
ε_o = 0.2%
FFC free
α = 0.042
ε_o = 0%
Drizzle Formation
Threshold
$D_{p,dry}$ = 10 μm
(a)

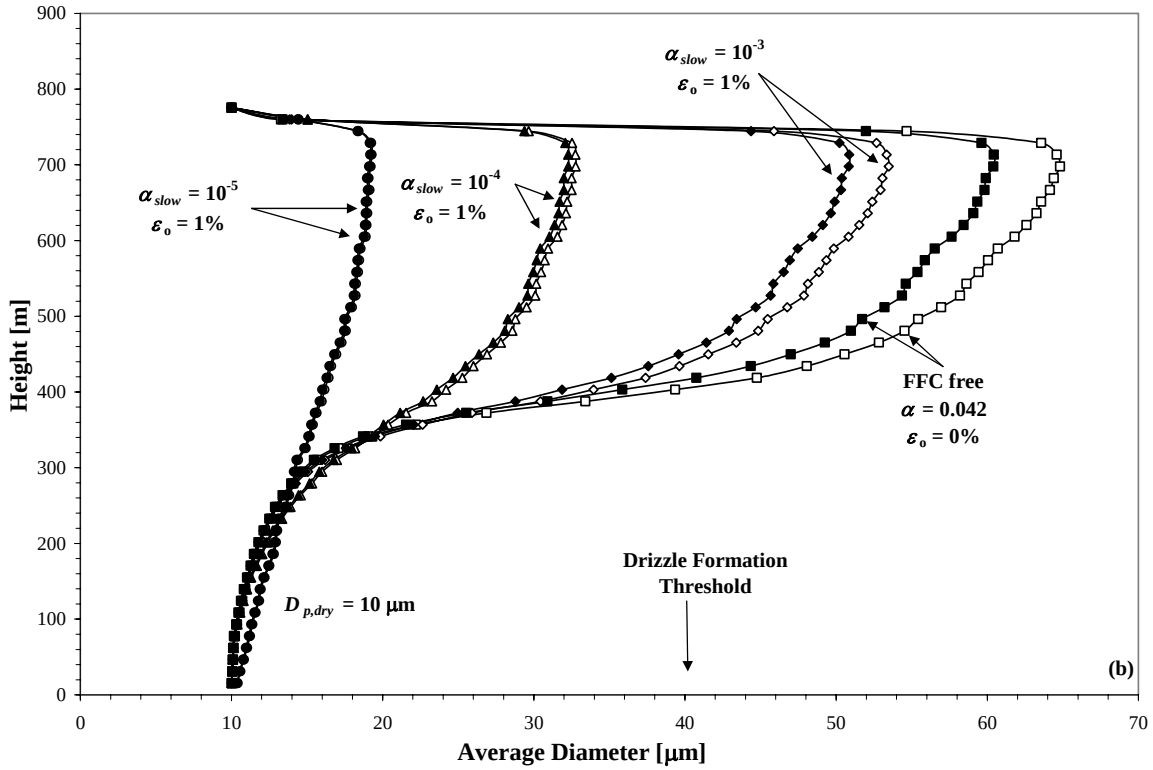
Height [m]
Average Diameter [μm]
α_{slow} = 10^{-3}
ε_o = 1%
α_{slow} = 10^{-5}
ε_o = 1%
α_{slow} = 10^{-4}
ε_o = 1%
FFC free
α = 0.042
ε_o = 0%
Drizzle Formation
Threshold
$D_{p,dry}$ = 10 μm
(b)

FIGURE 10.

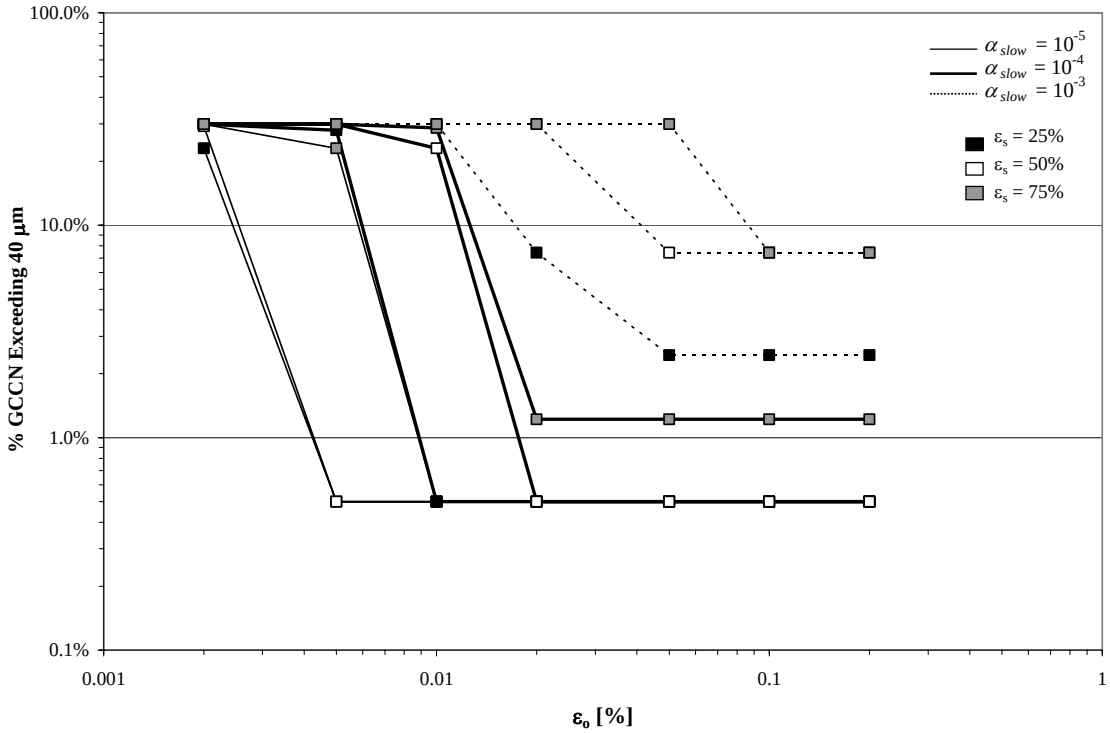
100.0%
10.0%
1.0%
0.1%
% GCCN Exceeding 40 µm
0.001
0.01
0.1
1
ε₀ [%]
α slow = 10-5
α slow = 10-4
α slow = 10-3
εs = 25%
εs = 50%
εs = 75%

FIGURE 11.